# Frontal waves in a strait

## MELVIN E. STERN AND JULIAN A. SIMEONOV

Department of Oceanography, Florida State University, Tallahassee, FL 32306-4320, USA
stern@ocean.fsu.edu; simeonov@ocean.fsu.edu

The slow downstream ($x$) variation of a dense and inviscid bottom current ($u$) in a parabolic strait with a sill at $y = 0$ is investigated. Vanishing potential vorticity is assumed and the density interface in the 1 1/2-layer model intersects the bottom at $y = y_1$ and $y = y_2 < y_1$, where the vanishing layer thickness ($h$) provides the free dynamical boundary condition. For time-dependent finite-amplitude waves, the nonlinear hyperbolic equations obtained here give the wave velocity and indicate the sense in which lateral wave steepening occurs. The long-wave perturbations of $y_1(x, t)$, $y_2(x, t)$ are stationary if

$$\frac{y_1}{y_2} = 1 - \frac{2}{1 + \sqrt{6g'\mu/f^2}}$$

where $g'$ is the reduced gravity, $\mu = \partial^2 M/\partial y^2$ is the parabolic curvature of the bottom elevation ($M$), and $f$ is the Coriolis parameter. This controls the upstream–downstream flow, and the downstream nonlinearity generates 'short' waves which may initiate lateral mixing with the adjacent (less dense) water mass.

It is also shown that short waves are exponentially amplified with a maximum growth rate (about 1/day) depending only on $g'\mu/f^2$. When $g'\mu/f^2 = 1$ (a narrow strait) the instability is suppressed, but for small $g'\mu/f^2 \ll 1$ the growth rate is comparable to the flat bottom case $\mu = 0$, studied by Griffiths, Killworth & Stern (*J. Fluid Mech.* Vol. 117, 1982, p. 343.).

## 1. Introduction

The Denmark Straits and the Faroe Island Straits are examples of relatively narrow and shallow passageways through which the coldest waters in the North Atlantic flow southward, thereby maintaining the deep water temperature (Borenäs & Lundberg 1988; Käse & Oschiles 2000; Girton & Sanford 2002; Käse, Girton & Sanford 2003). The mean flow upstream of the sill is notably different from further downstream. This suggests either a 'branch point' effect at the sill which controls the discharge (Whitehead, Leetmaa & Knox 1974; Whitehead 1998), or a resonant amplification of long quasi-stationary waves. Shorter scales generated by nonlinear frontal steepening (Stern 1980) can be subsequently amplified by the ageostrophic instability of Griffiths, Killworth & Stern (1982, henceforth referred to as GKS) and this may explain the formation of 'round' eddies in the downstream flow (see Pratt & Helfrich 2007). Recent observations (Geyer *et al.* 2006), numerical modelling (Ezer 2006) and laboratory experiments (Cenedese *et al.* 2004) indicate that the downstream flow near the sill may also be dominated by regular wave oscillations.

A great simplification in the dynamical problem occurs if the bottom water has vanishing potential vorticity (Whitehead *et al.* 1974; Stern 1980) and is slowly varying in
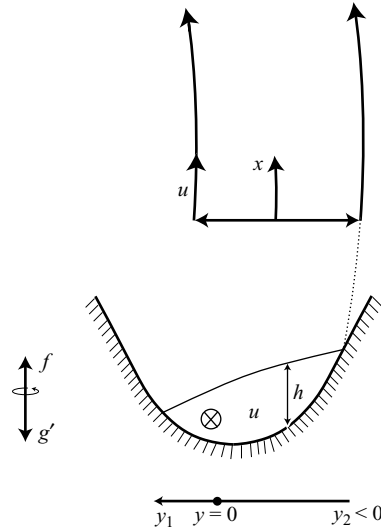
FIGURE 1. (*a*) Vertical section of a parabolic channel containing a slowly varying geostrophic flow (*u*) with a density interface, above which the liquid is light and resting. The free boundaries $y_1$, $y_2$ may vary slowly in the downstream direction. The sill is at $y = 0$.

the downstream ($x$) direction. Furthermore, laboratory experiments (Whitehead *et al.* 1974) employ straits with a rectangular cross-section, so that the relatively simple boundary condition of vanishing normal velocity applies. The main goal of that work (Whitehead *et al.* 1974) was to predict the volume discharge ($Q$) as a function of the upstream layer thickness using Bernoulli invariance.

Gill (1977) extended this theory by assuming a finite constant potential vorticity. This, in turn, was generalized by Borenäs & Lundberg (1986) who considered a parabolic channel with elevation $M = \mu y^2$, in which case the interface bounding the density current intersects the bottom at $y = y_1$ and $y = y_2$ (figure 1), where $h(y_1) = h(y_2) = 0$ provides the *free* boundary conditions. This $h$-structure is obviously a much more realistic representation of the isotherms at the bottom of oceanic straits (Girton, Sanford & Käse 2001). Unfortunately, however, the algebra in the Borenäs & Lundberg (1986) theory for finite potential vorticity is intractable, and therefore we want to return to the problem of flow with *vanishing* potential vorticity. This is done by Borenäs & Lundberg (1988) who maximize the transport to obtain the hydraulically 'controlled' flow. One criticism of the theory is that it is restricted to unidirectional flow.

Like the previous theories we assume a deep and passive upper layer (cf. Karsten, Swaters & Thomson 1995) and neglect bottom friction. The steady model of Borenäs & Lundberg (1988) is generalized by including time-dependent effects and downstream variation of topography. In addition to the question of what controls the volume transport

$$Q = \int_{y_1}^{y_2} uh \, \mathrm{d}y,$$

the time-dependent problem is also of interest since the *'lateral breaking'* of long free waves can lead to stronger cross-stream velocity $v$ which entrains the relatively light surrounding water, thereby initiating the increased downstream transport of the overflow. These time-dependent nonlinear long-wave equations for $y_1$ and $y_2$ are

obtained in §2. In §3, we use the method of characteristics to obtain finite-amplitude solutions of the long-wave equations. The short-wave instability linear theory of GKS for a flow on a uniform slope is extended in §4 for a channel with parabolic cross-section. The results are discussed in §5.

## 2. Long-wave equations in a parabolic channel

Figure 1 is a vertical section of a bottom density current (cf. Borenäs & Lundberg 1988) $u$ in a channel whose parabolic elevation is $M(x, y) = \mu y^2 + m(x)$, where $\mu$ is the constant cross-steam ($y$) curvature and $m(x)$ is the minimum $M$ at downstream distance $x$; the sill is at $m(x) = 0$. For slow downstream variations (figure 1) in a flow ($u$) with vanishing potential vorticity, the long-wave approximation ($\partial/\partial x \ll \partial/\partial y$) yields $\partial u/\partial y \cong f$, where $u \cong -g'/f \, \partial(h + M)/\partial y$ is the geostrophic down-channel ($x$) velocity, $g'$ is the reduced gravity of the lower layer, $h$ is its local depth, $f$ is the Coriolis parameter, and the cross-stream velocity is $v \ll u$. A straightforward integration yields

$$u = fy + a(x, t), \tag{1}$$

$$-\frac{\partial h}{\partial y} = f^2 y/g' + fa/g' + 2\mu y, \tag{2}$$

where $a$ is the constant in the integration of the vorticity equation. By using the free boundary conditions $h(y_1) = h(y_2) = 0$ in the integration of (2) in $y_2 \leqslant y \leqslant y_1$ we obtain

$$a = -f(y_1 + y_2)(\tfrac{1}{2} + G), \tag{3}$$

where

$$G \equiv \frac{g'\mu}{f^2}. \tag{4}$$

Figure 1 indicates that $y_2 < 0$, and therefore $a > 0$. Integrating (2) to finite $y$ yields

$$-h = \tfrac{1}{2}(f^2/g' + 2\mu)(y^2 - y_1^2) + (fa/g')(y - y_1). \tag{5a}$$

Note that $2u(y_2) = -f(y_1 - y_2) - (y_1 + y_2)2Gf \geqslant 0$ only if

$$\frac{-(y_1 + y_2)}{y_1 - y_2} \leqslant 2G. \tag{5b}$$

To illustrate: if $u(y_2) = 0$ and $-y_1/y_2 = 1/2$ then $2G = 1/3$. Equation (5b) restricts the applicability of zero potential vorticity profiles to one-way flow in a channel (Borenäs & Lundberg 1986). In the present theory no restriction is placed on the signs of $u(y_2, t)$.

Another important simplification of the long-wave model with vanishing potential vorticity lies in the $x$-momentum equation:

$$\frac{\partial u}{\partial t} + \frac{\partial}{\partial x}\left(\frac{u^2}{2} + g'h\right) + g'\frac{\partial m}{\partial x} = 0. \tag{6}$$

Using again (1) and (5a) we have

$$\frac{u^2}{2} + g'h = \frac{a^2}{2} + \frac{f^2 y^2}{2} - f^2 y^2(G + \tfrac{1}{2}) + f^2 y_1^2(G + \tfrac{1}{2}) + fay_1, \tag{7}$$

in which the $x$- and $y$-dependent terms are separated. Since the $x$-derivative of the $y$-dependent terms vanishes, (6) becomes

$$\frac{\partial a}{\partial t} + \frac{\partial}{\partial x}\left[\frac{a^2}{2} + fay_1 + f^2 y_1^2\left(G + \tfrac{1}{2}\right)\right] = -g'\frac{\partial m}{\partial x}. \tag{8}$$

Defining

$$D \equiv y_1 + y_2 < 0, \quad W \equiv y_1 - y_2 > 0, \tag{9}$$

where $W(x, t)$ is the distance between the two interfaces and $D < 0$ depends on the relative position of the sill, and eliminating $a = -fD(1/2 + G)$ from (3), (8) becomes

$$\boxed{-\frac{1}{f}\frac{\partial D}{\partial t} + \frac{\partial}{\partial x}\left(\frac{W^2}{4} + \frac{GD^2}{2}\right) = -g'\frac{\partial m}{\partial x}\frac{1}{f^2(G + 1/2)}}. \tag{10}$$

To obtain another equation for $(y_1, y_2)$ we turn to the continuity equation

$$\frac{\partial}{\partial t}\int_{y_2}^{y_1} h\,\mathrm{d}y + \frac{\partial Q}{\partial x} = 0. \tag{11}$$

Eliminating $u = fy + a$ from (1) in the mean downstream transport $Q \equiv \int_{y_2}^{y_1} uh\,\mathrm{d}y$ and integrating by parts (using $h = 0$ at $y = y_{1,2}$) gives

$$Q = -\int_{y_2}^{y_1}\left(\frac{fy^2}{2} + ay\right)\frac{\partial h}{\partial y}\,\mathrm{d}y.$$

Using (2), the integration yields

$$Q = -\frac{\mu}{6}\left(G + \tfrac{1}{2}\right)(y_1 - y_2)^3(y_2 + y_1)f. \tag{12}$$

To obtain the first term in (11) we first note that (5a) is equivalent to

$$-h = \frac{f^2}{g'}\left(\tfrac{1}{2} + G\right)[(y - y_1)^2 + (y_1 - y_2)(y - y_1)].$$

Changing the integration variable to $(y - y_1)$ we have

$$\int_{y_2}^{y_1} h\,\mathrm{d}y = -\frac{f^2}{g'}\left(G + \tfrac{1}{2}\right)\left[\frac{(y - y_1)^3}{3}\bigg|_{y_2}^{y_1} + (y_1 - y_2)\frac{(y - y_1)^2}{2}\bigg|_{y_2}^{y_1}\right], \tag{13}$$

or

$$\int_{y_2}^{y_1} h\,\mathrm{d}y = \frac{f^2}{g'}\left(G + \tfrac{1}{2}\right)\frac{W^3}{6}. \tag{14}$$

Then (11) becomes

$$\frac{1}{f}\frac{\partial}{\partial t}\frac{W^3}{6} - \frac{G}{6}\frac{\partial}{\partial x}(DW^3) = 0. \tag{15}$$

For $G > 0$ (10) and (15) are hyperbolic long-wave equations (for a given downstream variation of min $M = m$).

It is of interest to compare the transport $Q$ (equation (12)) with a purely geostrophic value appropriate for vertical boundaries:

$$Q_0 \equiv \frac{g'(M^2(y_2) - M^2(y_1))}{2f} = \frac{g'M^2(y_2)}{2f}(1 - \varepsilon^4),$$
$$\varepsilon \equiv y_1/y_2. \tag{16a}$$

This is closely related to the Whitehead *et al.* (1974) value. On the other hand, for the parabolic wall (12) gives

$$Q = \frac{f}{6}\mu y_2^4(1-\varepsilon)^3(1+\varepsilon)(G+1/2) = Q_0\left[\frac{G+1/2}{3G}\right]\frac{(1-\varepsilon)^2}{(1+\varepsilon^2)}. \tag{16b}$$

This shows the influence of $G = \mu g'/f^2$ on the transport, and it only remains to predict $\varepsilon$ or $W/D$.

## 3. Large-amplitude long waves

### 3.1. *Special solutions*

The general solutions of the initial value problem for the $2\times 2$ system (equations (10) and (15)) can be obtained from the two Riemann invariants once the two sets of characteristics are determined. Here, however, we are interested in the special case when one of the Riemann invariants is uniform and therefore the problem can be solved using only the set of characteristic lines corresponding to the second Riemann invariant. The condition that one of the Riemann invariants is uniform is equivalent to assuming that

$$D = D(W).$$

Using

$$\frac{\partial D}{\partial t} = D_W\frac{\partial W}{\partial t}, \quad \frac{\partial D}{\partial x} = D_W\frac{\partial W}{\partial x}, \quad D_W = \frac{\mathrm{d}D}{\mathrm{d}W}$$

and assuming $m = 0$, (10) and (15) become

$$\frac{1}{f}D_W\frac{\partial W}{\partial t} = \frac{W}{2}\frac{\partial W}{\partial x} + GDD_W\frac{\partial W}{\partial x}, \tag{171a}$$

$$\frac{1}{f}\frac{W^2}{2}\frac{\partial W}{\partial t} = \frac{G}{6}W^3D_W\frac{\partial W}{\partial x} + \frac{GD}{2}W^2\frac{\partial W}{\partial x}. \tag{172b}$$

The solvability condition obtained by dividing these equations yields

$$D_W = \pm\left(\frac{3}{2G}\right)^{1/2}. \tag{18}$$

The corresponding nonlinear phase speeds obtained from (17a) are

$$C_{\mp} \equiv -\frac{\partial W/\partial t}{\partial W/\partial x} = fG\left(-D \mp \frac{W}{\sqrt{6G}}\right). \tag{19}$$

Note that the phase speeds of the linearized hyperbolic equations (10), (15) are given by the same formula (19) except that $D$ and $W$ are replaced by their undisturbed values. The solutions with the '+' and '−' signs in (19) will be referred to as the fast wave and slow wave, respectively, since $C_+ > C_-$. While the fast wave always propagates downstream ($C_+ > 0$), the slow wave may be stationary ($C_- = 0$) or propagate upstream if

$$W \geqslant -D\sqrt{6G}. \tag{20}$$

The condition that the local propagation velocity vanishes corresponds to a critical section which determines the 'controlled' flow. Using

$$\frac{W}{D} \equiv \frac{y_1 - y_2}{y_1 + y_2} = -\frac{1-\varepsilon}{1+\varepsilon},$$

the equal sign in (20) suggests

$$\varepsilon = 1 - \frac{2}{1 + \sqrt{6G}}. \tag{21}$$

For given $G$, this $\varepsilon$ determines the transport (16$b$) which corresponds to a controlled flow. This should be compared with Borenäs & Lundberg (1988) who obtained the critical condition $W = -D\sqrt{6G}$ by maximizing $Q$ with respect to $W$. When $W$ is smaller than the critical value $-D\sqrt{6G}$ both waves (19) propagate downstream and this corresponds to a supercritical flow.

### 3.2. *Initial value solutions*

Here we will use the special solutions (18), (19) to investigate the nonlinear evolution of finite-amplitude perturbations which may lead to wave steepening. We assume an initial long-wave perturbation, corresponding to a localized (near $x = 0$) increase of the width of the flow:

$$\frac{W_0(x)}{W_\infty} = 1 + \frac{A/W_\infty}{1 + (x/L_*)^2}, \tag{22}$$

where $W_\infty$ is the upstream $x = -\infty$ ('undisturbed') width, $L_* \gg W_0$ is the downstream length of the perturbation and $A > 0$ is the perturbation amplitude. Equation (18) gives the initial $D_0(x)$ for the fast and the slow special solutions corresponding to (22):

$$D_0(x) - D_\infty = \pm\sqrt{\frac{3}{2G}}[W_0(x) - W_\infty]. \tag{23}$$

To obtain the solutions at subsequent times we first note that since $D$ and $W$ are conserved along the characteristic curves:

$$\frac{\mathrm{d}x}{\mathrm{d}t} \equiv C_\mp, \tag{24}$$

the phase speeds $C_\mp$ in (19) are also conserved along $x(t)$. The characteristic curves then are just straight lines

$$x = x_0 + C_\mp t, \tag{25}$$

where $x_0$ is the initial coordinate of a given width $W_0$. The solution then is

$$W(x, t) = W_0(x_0) = W_0(x - C_\mp t), \tag{26a}$$
$$D(x, t) = D_0(x_0) = D_0(x - C_\mp t). \tag{26b}$$

The corresponding displacements (normalized by $W_\infty$) of the two fronts

$$\frac{y_1(x, t)}{W_\infty} = \frac{D_0(x_0) + W_0(x_0)}{2W_\infty}, \quad \frac{y_2(x, t)}{W_\infty} = \frac{D_0(x_0) - W_0(x_0)}{2W_\infty}$$

are completely determined from (22), (23) and (26$a$, $b$) for given $G$, upstream condition $D_\infty/W_\infty$ and amplitude $A/W_\infty$. These are shown in figure 2 for $G = 0.5$, a subcritical upstream $-D_\infty/W_\infty = 1/3 < (6G)^{-1/2} = 3^{-1/2}$ and initial amplitude $A/W_\infty = 1/6$. The downstream-propagating fast solution (figure 2$a$) is characterized by a stronger displacement of the right-hand front $y_2$ while the displacement of the left-hand front $y_1$ is larger in the slow wave (figure 2$b$). For the present subcritical $D_\infty/W_\infty$, both solutions steepen at the leading edge of the wave. For supercritical conditions (larger $|D_\infty|$), however, the slow wave propagates downstream and the steepening occurs in the trailing edge. The present results indicate a forward steepening of the right-hand front and backward steepening of the left-hand front for supercritical flows. Similar
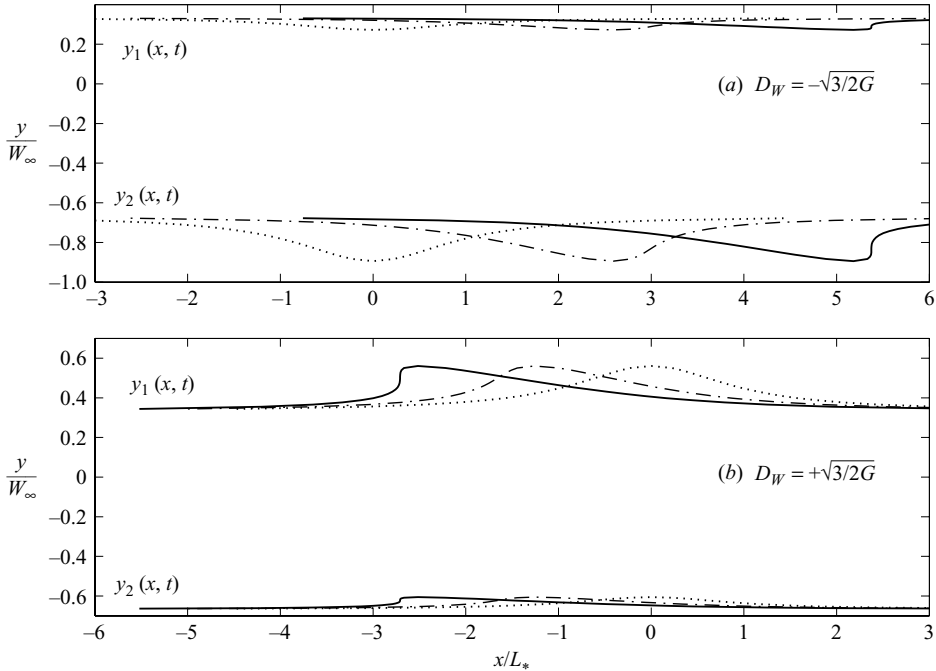
FIGURE 2. The evolution of a localized width bulge in the fast ($a$) and the slow ($b$) special solutions illustrated by the displacements of the two fronts $y_1$, $y_2$ at three different non-dimensional times $ftW_\infty/L_* = 0$ (dots), $ftW_\infty/L_* = 4$ (dash-dot) and $ftW_\infty/L_* = 8$ (solid). The bottom curvature corresponds to $G = 0.5$, the upstream flow is subcritical $-D_\infty/W_\infty = 1/3$, and the perturbation amplitude is $A/W_\infty = 1/6$. The cross-stream ($y$) and the downstream ($x$) coordinates are non-dimensionalized by $W_\infty$ and $L_*$.

wave-steepening is observed downstream of the sill in the numerical simulations of Pratt, Helfrich & Chassignet (2000) and Ezer (2006, his figure 6$d$).

The wave steepening can be easily explained by considering the downstream variation of the phase speed which according to (19) is

$$\frac{dC_\mp}{dx} = fG\left(-\frac{dD}{dx} \mp \frac{1}{\sqrt{6G}}\frac{dW}{dx}\right).$$

Using (18) to eliminate $dD/dx$ we obtain

$$\frac{dC_\mp}{dx} = \mp f\sqrt{\frac{8G}{3}}\frac{dW}{dx}.$$

This shows that the phase speed has an extremum at the section of maximum width; since $d^2W/dx^2 < 0$ at this section, the extremum is a maximum for $C_+$ and a minimum for $C_-$. Accordingly, for the fast solution, the section of maximum width overtakes any downstream section and the wave steepens forward. For the slow solution and supercritical conditions, the section of maximum width (having the smallest downstream $C_-$) is overtaken by faster moving upstream sections and the wave steepens backwards.

We also note that the displacement of the left front (figure 2$b$, see also (23)) in the slow wave results in a decrease of the local $|D(x)|$. If the amplitude $A$ is sufficiently large so that $|D(x)| = 0$ at some $x$, the upstream flow is 'blocked' as the total downstream transport $Q$ (12) would vanish at this section. Note that for a

general initial disturbance, the maximum amplitude is not conserved but may increase in time (cf. Stern 1980), giving rising to the blocking effect.

## 4. Short-wave instability

The results in the previous section indicate that short-wave disturbances will be rapidly generated due to the steepening of long-wave perturbations. Here we will investigate the effect of short waves by extending the linear stability theory of GKS, for a bottom gravity current $\bar{u}$ in a parabolic channel. The mean flow in (1), (5a) is assumed independent of the downstream ($x$) direction and the left-hand and the right-hand (viewing downstream) free edges where the layer thickness vanishes are denoted by $\bar{y}_1$ and $\bar{y}_2$, respectively. Our focus is on the fastest growing instability; a more detailed study of this stability problem which includes non-GKS instability can be found in Pratt & Helfrich (2007).

The basic state is next perturbed by infinitesimal waves with velocities $u'(x, y, t)$, $v'(x, y, t)$, and depth $h'$, whose downstream wavelength is comparable to the mean width $\bar{y}_1 - \bar{y}_2$. Accordingly, we reinstate the $x$-derivative in the conservation of potential vorticity (assumed to be initially zero):

$$\partial u'/\partial y - \partial v'/\partial x = 0; \tag{27a}$$

this implies that the considered wave perturbations are irrotational. The problem is closed with the linearized continuity

$$\frac{\partial h'}{\partial t} + \bar{u}\frac{\partial h'}{\partial x} + \bar{h}\frac{\partial u'}{\partial x} + \frac{\partial v'\bar{h}}{\partial y} = 0 \tag{27b}$$

and $x$-momentum equations

$$\frac{\partial u'}{\partial t} + \bar{u}\frac{\partial u'}{\partial x} = -g'\frac{\partial h'}{\partial x}. \tag{27c}$$

Note the cancellation of $v'\partial\bar{u}/\partial y - fv' = 0$ in (27c).

Introducing the function $\Psi$, such that

$$u' \equiv \partial\Psi/\partial x, \quad v' \equiv \partial\Psi/\partial y, \tag{27d}$$

and assuming normal modes $[u', v', \Psi', h'] = \mathrm{Re}([\hat{u}(y), \hat{v}, \hat{\Psi}, \hat{h}]\mathrm{e}^{\mathrm{i}k(x-ct)})$ equations (27) yield the following ODE for $\hat{\Psi}$:

$$\frac{\mathrm{d}}{\mathrm{d}y}\left(\bar{h}\frac{\mathrm{d}\hat{\Psi}}{\mathrm{d}y}\right) - k^2\left[\bar{h} - \frac{(\bar{u}-c)^2}{g'}\right]\hat{\Psi} = 0. \tag{28}$$

Evaluating (28) at $y = \bar{y}_{1,2}$ where $\bar{h} = 0$ gives the two boundary conditions

$$\frac{\mathrm{d}\bar{h}}{\mathrm{d}y}\frac{\mathrm{d}\hat{\Psi}}{\mathrm{d}y} + k^2\left[\frac{(\bar{u}-c)^2}{g'}\right]\hat{\Psi} = 0, \quad \text{at } y = \bar{y}_{1,2} \tag{29a}$$

relating $\mathrm{d}\hat{\Psi}/\mathrm{d}y$ and $\hat{\Psi}$ at the free edges. These boundary conditions can be formally derived using two conditions: (i) that the frontal boundaries are material and (ii) that the gradient of $(\bar{h} + h')$ at the boundaries has vanishing component in the tangential direction. One of the boundary conditions (29a) can be replaced by an integral condition (cf. GKS) obtained by integrating (28) in $\bar{y}_2 \leqslant y \leqslant \bar{y}_1$:

$$\int_{\bar{y}_2}^{\bar{y}_1}\left[\bar{h} - \frac{(\bar{u}-c)^2}{g'}\right]\hat{\Psi}\,\mathrm{d}y = 0. \tag{29b}$$

For comparison with the long-wave theory of §3, we expand (following GKS) both $\hat{\Psi}$ and $c$ in power series of an infinitesimal $k$. Equation (28) then suggests that the zeroth-order term $\hat{\Psi}_0$ is constant and the integral (29b) then gives a quadratic equation for $c_0$. The phase speeds predicted by this quadratic for $k \to 0$ are the same as those in equation (19).

### 4.1. *Dependence on $\bar{y}_1$, $\bar{y}_2$ and G.*

We will now transform the eigenvalue problem (28), (29) to show that the growth rate $\sim \mathrm{Im}(c)$ does not depend on the location of the centroid $\bar{D}/2 \equiv (\bar{y}_1 + \bar{y}_2)/2$ relative to the sill. Using the identities

$$\bar{y}_1 = \frac{\bar{W}}{2} + \frac{\bar{D}}{2}, \quad \bar{y}_2 = -\frac{\bar{W}}{2} + \frac{\bar{D}}{2}, \tag{30}$$

where $\bar{W}/2 \equiv (\bar{y}_1 - \bar{y}_2)/2$, the mean velocity $\bar{u}$ (1) and thickness $\bar{h}$ (5) become

$$\bar{u} = fy - f\left(\tfrac{1}{2} + G\right)\bar{D} = f(y - \bar{D}/2) - fG\bar{D}, \tag{31a}$$

$$\bar{h} = -\frac{f^2}{g'}\left(G + \tfrac{1}{2}\right)[(y - \bar{D}/2)^2 - \bar{W}^2/4]. \tag{31b}$$

Transforming the cross-stream coordinate $y - \bar{D}/2 \to y$ so that the new origin $(y = 0)$ is at the centroid and substituting (31a, b) in (28) gives

$$\frac{\mathrm{d}}{\mathrm{d}y}\left(\left(\frac{\bar{W}^2}{4} - y^2\right)\frac{\mathrm{d}\hat{\Psi}}{\mathrm{d}y}\right) - k^2\left[\left(\frac{\bar{W}^2}{4} - y^2\right) - \frac{(fy - fG\bar{D} - c)^2}{f^2\left(G + \tfrac{1}{2}\right)}\right]\hat{\Psi} = 0. \tag{32}$$

Similarly, the integral condition (29b) becomes

$$\int_{-\bar{W}/2}^{\bar{W}/2}\left[\left(\frac{\bar{W}^2}{4} - y^2\right) - \frac{(fy - fG\bar{D} - c)^2}{f^2\left(G + \tfrac{1}{2}\right)}\right]\hat{\Psi}\,\mathrm{d}y = 0. \tag{33}$$

In (32) and (33), the parameter $\bar{D} \equiv (\bar{y}_1 + \bar{y}_2)$ now enters only as an additive constant to the eigenvalue $c$. Thus, the transformed eigenvalue $\tilde{c}$:

$$\tilde{c} \equiv c + fG\bar{D}, \tag{34}$$

is independent of the centroid location $\bar{D}/2$. Because $\mathrm{Im}(c) = \mathrm{Im}(\tilde{c})$, the growth rate of the original problem is also independent of $\bar{D}/2$ and the latter only affects (linearly) the phase speed $\mathrm{Re}(c)$ of the eigenmode.

To illustrate the dependence on the half-width $\overline{W} \equiv (\bar{y}_1 - \bar{y}_2)$ we note that under the scaling

$$(k^{-1}, y) = \left(k_0^{-1}, y_0\right)\bar{W}/2, \quad \tilde{c} = \tilde{c}_0 f \frac{\bar{W}}{2}\left(G + \tfrac{1}{2}\right)^{1/2}, \tag{35}$$

equations (32) and (33) become independent of $\bar{W}$:

$$\frac{\mathrm{d}}{\mathrm{d}y_0}\left((1 - y_0^2)\frac{\mathrm{d}\hat{\Psi}}{\mathrm{d}y_0}\right) - k_0^2\left[(1 - y_0^2) - \left(\frac{y_0}{\sqrt{G + \tfrac{1}{2}}} - \tilde{c}_0\right)^2\right]\hat{\Psi} = 0, \tag{36}$$

$$\int_{-1}^{1}\left[(1 - y_0^2) - \left(\frac{y_0}{\sqrt{G + \tfrac{1}{2}}} - \tilde{c}_0\right)^2\right]\hat{\Psi}\,\mathrm{d}y_0 = 0. \tag{37}$$

Thus, the wavelength and the phase speed of the perturbations are proportional to the width of the current $\overline{W}$. The growth rate $\mathrm{Im}(kc) = (G + 1/2)^{1/2} f\,\mathrm{Im}(k_0\tilde{c}_0)$,

however, is independent of $\overline{W}$, and according to (36) and (37) depends on a single non-dimensional parameter $G$. We note that the factor $(G + 1/2)^{1/2}$ used to scale $\tilde{c}$ comes from the speed of long gravity waves based on the maximum current thickness $f^2\overline{W}^2(G + 1/2)/4g'$ (see (31b)).

Next, we discuss the dependence of the growth rate on $G$. For $G = 0$, the eigenvalue problem (36) and (37) is equivalent to the one in GKS and therefore we are assured of the existence of growing solutions with finite growth rate for $G = 0$. The growth rate, however, might be greatly reduced when $G$ is large as the boundary conditions become more like those in a channel with vertical walls. This can be illustrated by considering the asymptotic limit $G \to \infty$ and retaining terms to $O(G^{-1/2})$ in the ODE (36). The resulting ODE is then multiplied by the complex conjugate $\hat{\Psi}^*$ and integrated in $-1 \leqslant y \leqslant 1$ to obtain two conditions for the real and the imaginary part. It can be shown that these two conditions can be satisfied only when $\mathrm{Im}(\tilde{c}) = 0$ (to $O(G^{-1/2})$). The question whether the growth rate vanishes identically if $G$ exceeds a certain critical value is addressed by the numerical solutions in the next section.

### 4.2. Numerical solutions

In this section, we solve (36) and (37) numerically by assuming solutions in the form of a truncated power series expansion about the left-hand boundary $y_0 = 1$

$$\hat{\Psi}(y_0) = B \sum_{n=0}^{N} a_n \frac{(1 - y_0)^n}{2^n}, \tag{38}$$

where $B$ is a unspecified dimensional scale. Substitution of (38) in (36) yields a recursive formula relating $a_{n+1}$ to $a_n$, $a_{n-1}$ and $a_{n-2}$:

$$a_{n+1} = \frac{n(n+1) - \sigma^2}{(n+1)^2} a_n + \frac{4(k_0^2 - bk_0\sigma)}{(n+1)^2} a_{n-1} - \frac{4k_0^2(1 + b^2)}{(n+1)^2} a_{n-2}, \tag{39}$$

where $b \equiv (G + 1/2)^{-1/2}$, $\sigma \equiv k_0(\tilde{c}_0 - b)$ and $a_{-1} = a_{-2} = 0$. It is straightforward to show that the boundary condition (29a) at $y = \bar{y}_1$ – a relationship between $a_1$ and $a_0$ – is automatically satisfied when $a_1$ is related to $a_0$ by the recursive formula. The boundary condition (29a) at the other boundary $y = \bar{y}_2$ and the integral condition (29b), however, are automatically satisfied only for an infinite $N = \infty$ power series. Thus, for finite $N$, substitution of (38) into (37) yields a relationship for the two highest coefficients $a_N$ and $a_{N-1}$:

$$a_N \left[ \frac{b}{k_0(1 + b^2)} \sigma + \frac{N+2}{N+3} - \frac{1}{1 + b^2} \right] + a_{N-1} = 0; \tag{40}$$

the boundary condition at $y = \bar{y}_2$ results in similar formula except that the term $(N + 2)/(N + 3)$ is replaced by one.

Using $a_{-1} = a_{-2} = 0$, and assuming (without loss of generality) that $a_0 = 1$, equation (39) can be used to determine the higher coefficients $a_n$ as polynomials in $\sigma$ of degree $2n$ (for example, $a_1 = -\sigma^2$):

$$a_n = P_{2n}(\sigma). \tag{41}$$

The polynomials (41) for the two highest coefficients $a_N$ and $a_{N-1}$ then are substituted in (40) and this yields the characteristic polynomial for $\sigma$ as function of $k_0$, $G(b)$ and the truncation number $N$. All the roots of the characteristic polynomial are obtained using Matlab. Although this procedure usually yields many complex roots for given $k_0$ and $G$, we found only one pair of complex roots corresponding to a convergent
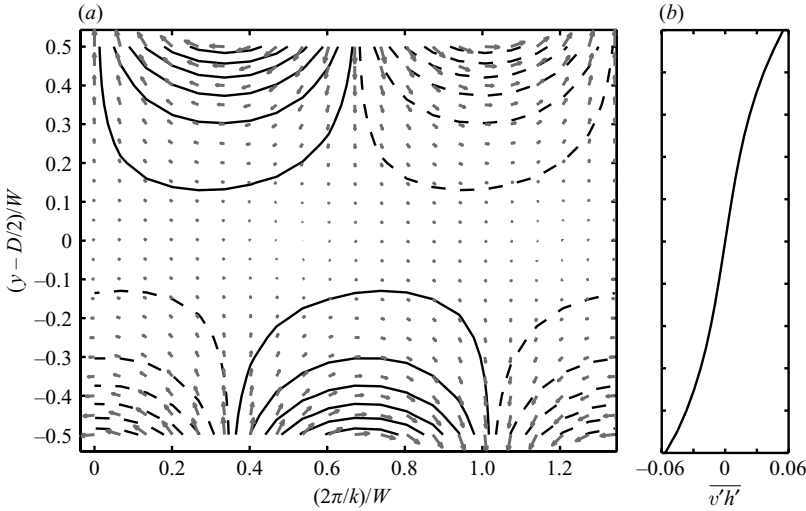
FIGURE 3. (*a*) The velocity field (grey arrows) and the thickness perturbation (contours) for the fastest growing normal mode for $G = 0.5$. Solid (dashed) contours denote positive (negative) perturbation thickness; these have their largest amplitude near $y - D/2 = \pm W/2$. (*b*) The average cross-stream mass flux $\overline{v'h'}$ corresponding to (*a*).

power series solution. The unphysical roots are filtered out by requiring $|a_N| \ll a_0 = 1$. Convergence of the eigenvalues to the fourth significant digit is typically obtained for $N = 30$.

Once the eigenvalue $\sigma$ is known, the coefficients in the power series solution (38) are obtained from (41). The corresponding velocity and thickness perturbations then are computed using (27*d*) and (27*c*). These are plotted in figure 3*a* for $G = 0.5$ and the corresponding fastest growing $k_0 = 2.34$ (below). The amplitude of the eigenfunction is maximum near the free boundaries, which is typical for GKS-type instability. It is also worth noting that the eigenfunction remains symmetric across the downstream axis despite the asymmetry introduced by the parabolic geometry (variable bottom slope). Because of this symmetry, the corresponding cross-stream mass flux $\overline{v'h'}$ (figure 3*b*) is antisymmetric and outwards from the centre. This flux would result in the lateral spreading of the plume as demonstrated in the laboratory experiments of GKS.

The largest growth rate at given $G$ is obtained by repeating the root-finding calculation for different $k_0$ and searching the results. As a test of the procedure we started with $G = 0$ for which the known (GKS) fastest growing wavenumber is $k_0 = 0.8\sqrt{2}$. The search is then repeated in the vicinity of this wavenumber by increasing the value of $G$. The dependence of the maximum dimensional growth rate $\mathrm{Im}(kc)$ on $G$ and the corresponding wavelength $2\pi/k$ are shown in figures 4(*a*) and 4(*b*), respectively. As expected, the growth rate decreases rapidly with increasing $G$ (or $\mu$). The slope of the curve in figure 4(*a*), however, decreases with increasing $G$ and indicates that the growth rate does not vanish at finite $G$. Figure 4(*b*) shows that the fastest growing wavelength $2\pi/k$ decreases with $G$; for comparison, we note that the deformation radius based on the maximum thickness $f^2 \bar{W}^2 (G + 1/2)/4g'$ (31*b*) increases as $(G + 1/2)^{1/2}$.

Figure 4(*a*) offers a strong proof that the instability of zero potential vorticity flow in a parabolic channel generalizes that of the corresponding flow on a flat bottom. In the latter case, Paldor (1983) showed that the instability is produced by
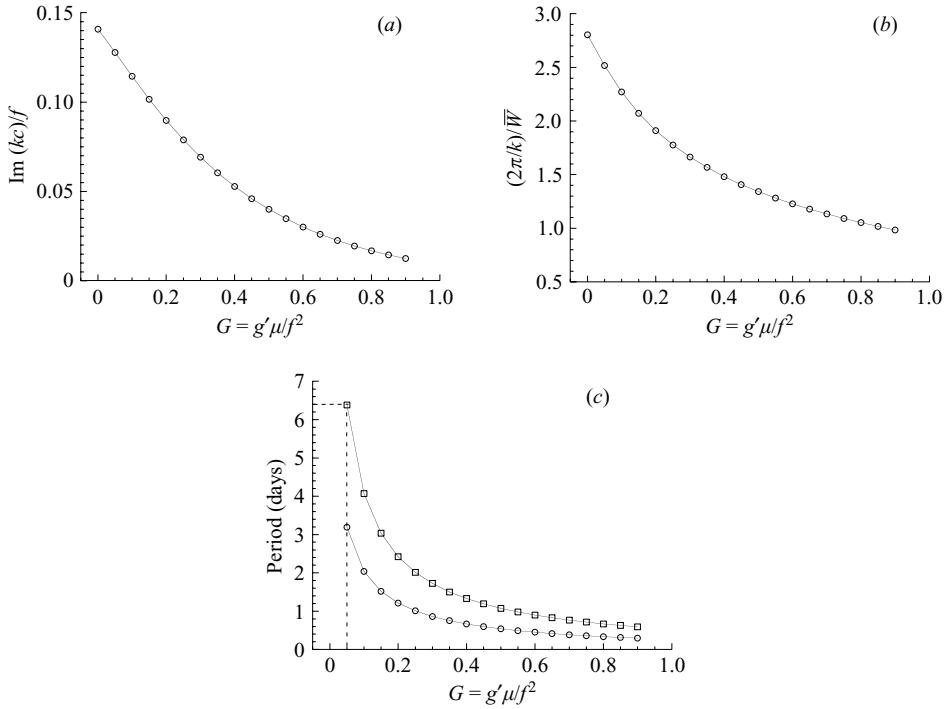
FIGURE 4. The growth rate (*a*), the wavelength (*b*) and the period $2\pi\bar{W}/(k_0|\bar{D}|fG)$ (*c*) of the fastest growing short wave as a function of $G$. The period in (*c*) is obtained by assuming $f = 10^{-4}\,\mathrm{s}^{-1}$, a critical flow (circles) with $\bar{W} = |\bar{D}|\sqrt{6G}$ and a subcritical flow (squares) with $\bar{W} = 2|\bar{D}|\sqrt{6G}$; the growth rate (*a*) and the wavelength (*b*) do not depend on $\bar{D}$.

the cooperation of the two free interfaces. With more general potential vorticity, we expect other types of shear flow modes to be generated.

Our numerical results also show that the fastest growing mode has $\mathrm{Re}(\tilde{c}_0) \approx 0$. From (34) and (35) we then obtain a simple expression for the phase speed of the fastest growing wave:

$$\mathrm{Re}(c) \approx -fG(\bar{y}_1 + \bar{y}_2), \qquad (42)$$

indicating that the latter travel with the mean current speed $\bar{u}$ at $y = (\bar{y}_1 + \bar{y}_2)/2$. Note that the speed (42) is the average $(C_+ + C_-)/2$ of the speeds of the fast and the slow special waves (19) of §3. The period of the oscillations corresponding to (42) is equal to the non-dimensional wavelength (figure 4*b*) multiplied by $\bar{W}/|\mathrm{Re}(c)| = \bar{W}/(|\bar{D}|fG)$. Assuming a critical flow with $\bar{W}/\bar{D} = -\sqrt{6G}$ (20) the dependence of this period on $G$ is shown in figure 4(*c*).

## 5. Conclusion

A parabolic channel is a much better representation of a narrow strait than is a rectangular section with a flat bottom; in the latter case the density interface intersects vertical walls at the points where vanishing normal velocity is the appropriate boundary condition. In the former case the appropriate free boundary condition yields a PDE (10), describing the slow downstream variation (long waves) of the free endpoints $y_1$, $y_2$. The second PDE (15) for these long frontal waves comes from the

conservation of mass. The main assumption of vanishing potential vorticity is used in simplifying the downstream momentum equation.

The channel curvature parameter $G = g'\mu/f^2$ is a fundamental non-dimensional number, and if $\mu < 0$ the evolutionary equation is elliptic implying that long waves on a shelf ($\mu < 0$) are unstable, which is also the case for $\mu = 0$ (GKS). But for the case of present interest ($\mu > 0$) the long-wave PDE is hyperbolic. 'Special' (Riemann waves) nonlinear solutions (§ 3) give the condition for one of the two waves to be stationary (20); the other wave propagates rapidly downstream. Unlike previous steady theories of controlled flow, we make no statement about the upstream boundary condition and only assume a stationary wave. The condition for a stationary wave relates the position of the interface ($y_1, y_2$) to the channel curvature $G$. This provides a criterion for control which, compared to Froude number criteria, is readily applied to observation.

Observations (Borenäs & Lundberg 1988) in the Faroe Straits yield $G = 1.5$ at the sill, and from their figure 5($a$), we estimate $y_1 = +4\,\text{km}$, $y_2 = -10\,\text{km}$, or $y_1/y_2 = -4/10$. Our theory (§ 3) on the other hand gives $W/(-D) = \sqrt{6G}$, or $y_1/y_2 = -1/2$, in very close agreement. Thus, we conclude that there are stationary waves near the Faroe sill, and this determines the transport as approximated by Borenäs & Lundberg.

The 'special' nonlinear solutions also indicate where long-wave steepening and amplifying transverse velocities ($v$) should occur. A reviewer raised the question of whether the long-wave steepening occurs on slower time scale compared to the e-folding time of unstable short waves. We have therefore generalized the GKS linear theory for a parabolic bottom and found that the growth rate depends only on the non-dimensional bottom curvature $G$ and decreases as $G$ increases (figure 4$a$). This growth rate can now be compared with the steepening rate of the special long waves of § 3.2. If we characterize the local steepness by the downstream derivative of the width $W_x$, we note that along the characteristics (25), the rate of change of a long wave $W_x$ is given by

$$\frac{1}{W_x}\frac{\mathrm{d}W_x}{\mathrm{d}t} = -\frac{\mathrm{d}C}{\mathrm{d}x} = \pm f\sqrt{\frac{8G}{3}}W_x. \qquad (43)$$

In contrast to this, the corresponding growth rate $W_x^{-1}\mathrm{d}W_x/\mathrm{d}t$ for the short-wave instability is constant in time. In a narrow channel with $G = 1$, figure 4($a$) suggests a short-wave growth rate of about $0.005f$. For a long-wave perturbation with initial (maximum) $W_x = 0.01$ equation (43) implies a 3 times larger initial growth rate ($0.016f$) of $W_x$; thus the long-wave dynamics will dominate. Further downstream where $G$ is much smaller, the shorter waves will grow faster (figure 4$a$) and will strongly affect a long-wave perturbation.

Ezer (2006) studied the influence of the sill geometry on the variability of the downstream flow using a high-resolution terrain-following ocean model. For parameters representative of the Faroe Bank Channel overflow, he found two regimes characterizing the flow downstream of the sill: regular wave perturbations with a period of 4–6 days near the sill and irregular eddies further downstream.

Our results suggest the following interpretation of Ezer's numerical simulations. In the narrow channel near the sill, the short-wave instability is weak (due to large $G$) and the dynamics is controlled by one nearly stationary and one downstream-propagating long wave. Short waves are nevertheless rapidly generated due to the nonlinear tendency of long waves to steepen. These short waves are subsequently amplified by the ageostrophic instability which becomes stronger (figure 4$a$) further downstream where $G$ is smaller. For $G = 0.05$ and critical $\bar{W}/|\bar{D}| \approx 0.5$, approximately

corresponding to a section in the wave regime of Ezer's calculations, figure 4(*c*) suggests a wave period of 3.2 days, in good agreement with observations (Geyer *et al.* 2006) and somewhat shorter than the period of 6.5 days obtained in Ezer's simulations.

For sufficiently large amplitudes lateral wave breaking may lead to entrainment of the more dense water into either side of the overflow. The lateral mixing in the outflow will be additionally affected by the formation of eddies due to the ageostrophic shortwave instability (Pratt & Helfrich 2007). These effects may be investigated numerically utilizing the complete (hydrostatic) equations and by initializing these with the 'special' long wave of the present theory. For a related numerical problem pertaining to coastal jets see Stern & Helfrich (2002), and Stern & Chassignet (2000).

## REFERENCES

BORENÄS, K. & LUNDBERG, P. 1986 Rotating hydraulics of flow in a parabolic channel. *J. Fluid Mech.* **167**, 309–326.

BORENÄS, K. M. & LUNDBERG, P. 1988 On the deep-water flow through the Faroe Bank Channel. *J. Geophys. Res.* **93**(C2), 1281–1292.

CENEDESE, C., WHITEHEAD, J. A., ASCARELLI, T. A. & OHIWA, M. 2004 A dense current flowing down a sloping bottom in a rotating fluid. *J. Phys. Oceanogr.* **31**, 1904–1914.

EZER, T. 2006 Topographic influence on overflow dynamics: Idealized numerical simulations and the Faroe Bank Channel overflow. *J. Geophys. Res.* **111**, C02002, doi:10.1029/2005JC003195.

GEYER, F., OSTERHUS, S., HANSEN, B. & QUADFASEL, D. 2006 Observations of highly regular oscillations in the overflow plume downstream of the Faroe Bank Channel. *J. Geophys. Res.* **111**, C12020, doi:10.1029/2006JC003693.

GILL, A. E. 1977 The hydraulics of rotating-channel flow. *J. Fluid Mech.* **80**, 641–671.

GIRTON, J. B. & SANFORD, T. B. 2002 A process study of the Denmark Strait Overflow. The 2nd Meeting on the Physical Oceanography of Sea Straits, Villefranche, 15–19 April 2002, pp. 107–111.

GIRTON, J. B., SANFORD, T. B. & KÄSE, R. H. 2001 Synoptic sections of the Denmark Strait overflow. *Geophys. Res. Lett.* **28**(8), 1619–1622.

GRIFFITHS, R. W., KILLWORTH, P. D. & STERN, M. E. 1982 Ageostrophic instability of ocean currents. *J. Fluid Mech.* **117**, 343–377.

KARSTEN, R. H., SWATERS, G. E. & THOMSON, R. E. 1995 Stability characteristics of deep-water replacement in the Strait of Georgia. *J. Phys. Oceanogr.* **25**, 2391–2403.

KÄSE, R. H., GIRTON, J. B. & SANFORD, T. B. 2003 Structure and variability of the Denmark Strait overflow: Model and observations. *J. Geophys. Res.* **108**(C6), 3181.

KÄSE, R. H. & OSCHLIES, A. 2000 Flow through Denmark Strait. *J. Geophys. Res.* **105**, 28527–28546.

PALDOR, N. 1983 Stability and stable modes of coastal fronts. *Geophys. Astrophys. Fluid Dyn.* **27**, 217–228.

PRATT, L. & HELFRICH, K. 2007 On the stability of ocean overflows. *J. Fluid Mech.* submitted.

PRATT, L. J., HELFRICH, K. R. & CHASSIGNET, E. P. 2000 Hydraulic adjustment to an obstacle in a rotating channel. *J. Fluid Mech.* **404**, 117–149.

STERN, M. E. 1980 Geostrophic fronts, bores, breaking and block waves. *J. Fluid Mech.* **99**(4), 687–703.

STERN, M. E. & CHASSIGNET, E. P. 2000 Mechanism of eddy separation from coastal currents. *J. Mar. Res.* **58**, 269–295.

STERN, M. E. & HELFRICH, K. 2002 Propagation of a finite-amplitude potential vorticity front along the wall of a stratified fluid. *J. Fluid Mech.* **468**, 179–204.

WHITEHEAD, J. A. 1998 Topographic control of oceanic flow in deep passages and straits. *Rev. Geophys.* **36**(3), 423–440.

WHITEHEAD, J. A., LEETMAA, A. & KNOX, R. A. 1974 Rotating hydraulics of strait and sill flows. *Geophys. Fluid Dyn.* **6**, 101–125.